Quantifying and modelling the impact of land consolidation and field borders on soil redistribution in agricultural landscapes (1954–2009)

Caroline Chartin, O. Evrard, Sébastien Salvador-Blanes, Florent Hinschberger, Kristof van Oost, Irène Lefèvre, Joël J. Daroussin, Jean-Jacques Macaire

Quantifying and modelling the impact of land consolidation and field borders on soil redistribution in agricultural landscapes (1954 – 2009)

Caroline Chartin[1,2], Olivier Evrard[2*], Sébastien Salvador-Blanes[1], Florent Hinschberger[1], Kristof Van Oost[3], Irène Lefèvre[2], Joël Daroussin[4], Jean-Jacques Macaire[1]

[1] *EA 6293 GéHCo (Géo-Hydrosystèmes Continentaux), EA 6293, Université François-Rabelais de Tours, Faculté des Sciences et Techniques, Parc de Grandmont, 37200 Tours (France)*

[2] *LSCE (Laboratoire des Sciences du Climat et de l'Environnement), UMR 8212(CEA-CNRS-UVSQ) Avenue de la Terrasse, 91198 Gif-sur-Yvette (France)*

[3] *TECLIM – Earth & Life Institute, Université catholique de Louvain, Place Louis Pasteur, 1348 Louvain-la-Neuve (Belgium)*

[4] *INRA – Unité de Science du Sol, 2163 avenue de la Pomme de Pin, CS 40001 Ardon, 45075 Orléans Cedex 2, France*

[*]**Corresponding author.** Tel.: +33 1 69 82 35 41; fax: +33 1 69 82 35 68.

E-mail address: caroline.chartin@lsce.ipsl.fr (C.Chartin)

Present address: *LSCE (Laboratoire des Sciences du Climat et de l'Environnement), UMR 8212 (CEA-CNRS-UVSQ) Avenue de la Terrasse, 91198 Gif-sur-Yvette (France)*

Abstract

Soil erosion rates in cultivated areas have intensified during the last decades leading to both on and off-site problems for farmers and rural communities. Furthermore, soil redistribution processes play an important role in sediment and carbon storage within, and exports from, cultivated catchments. This study focuses on the impact of land consolidation and changes in landscape structure on medium term soil erosion and landscape morphology within a 3.7-ha field in France. The area was consolidated in 1967 and we used the ^{137}Cs-technique to quantify soil erosion for the period (1954-2009). We measured the ^{137}Cs

inventories of 68 soil cores sampled along transects covering the entire area and especially specific linear landforms located along both present and past field borders (i.e., lynchets and undulations landforms, respectively). These results were then confronted with the outputs of a spatially-distributed ^{137}Cs conversion model that simulates and discriminates soil redistribution induced by water and tillage erosion processes. Our results showed that tillage processes dominated the soil redistribution in our study area for the last 55 years and generated about 95% (i.e., 4.50 $Mg.ha^{-1}.yr^{-}1$) of the total gross erosion in the field. Furthermore, we demonstrated that soil redistribution was largely affected by the presence of current and also former field borders, where hotspots areas of erosion and deposition (> 20 $Mg.ha^{-1}.yr^{-1}$) were concentrated. Land consolidation contributed to the acceleration of soil erosion through the conversion of depositional areas into sediment generating areas. Although the conversion model was able to reproduce the general tendencies observed in the patterns of ^{137}Cs inventories, the model performance was relatively poor with a r^2 of 0.20. Discrepancies were identified and associated with sampling points located along the current field borders. Our data suggests that tillage erosion processes near field boundaries cannot be described as a typical diffusive process. These processes near field boundaries should be characterised and taken into account in a future version of the model to accurately simulate rates and patterns of past soil redistribution in fragmented cultivated hillslopes. We also showed that the use of an accurate DEM resulting from LIDAR data, based on present-day topography, leads to the underestimation of soil redistribution rates by the model, especially in this landscape submitted to recent and important morphological changes. Our results have important implications for the simulation of tillage erosion processes and our understanding of soil redistribution processes in complex cultivated areas. This is of particular interest to improve our knowledge and prediction of patterns of soil physical parameters, such as carbon storage or water content, particularly sensitive to surface erosion and landscape structuration.

Keywords: Soil erosion; Field border; Land consolidation; Cesium-137; Conversion model; LIDAR

1. Introduction

During the last decades, soil erosion rates in cultivated areas of western Europe have intensified and have become a problematic issue for farmers and rural communities. When it is triggered by heavy storms, soil erosion and the associated muddy floods can have disastrous and costly consequences (e.g. Pimentel et al., 1995; Evrard et al., 2007a). Additional concerns about soil erosion are related to its subsequent negative impacts, such as water pollution, decline in biodiversity and crop yields or reduction of soil water storage capacity or organic carbon sequestration (e.g. Andraski and Lowery, 1992; Berger et al., 2006; Boardman and Poesen, 2006; Papiernick et al., 2009). Because soil is a non-renewable resource at human timescales, soil protection is crucial. Quantification of erosion and deposition rates and the identification of their driving processes and their spatial variability therefore constitute a prerequisite to develop and implement soil protection strategies.

Traditionally, soil redistribution processes observed on croplands in western Europe were mainly attributed to water erosion processes. In that case, transport intensity is controlled by topographical settings such as slope, drainage area and planform curvature (Poesen, 1984; Foster, 1986; Chaplot and Le Bissonnais, 2003). However, research has shown that tillage operations result in significant soil redistribution in intensively farmed cropland (e.g. Lindstrom et al., 1992; Govers et al., 1994). Tillage erosion results from the net downslope translocation of soil, controlled by slope gradient change, during farming operations (Lindström et al., 1990; Govers et al., 1994; Montgomery et al., 1999; Van Muysen et al., 1999). As shown by Govers et al. (1994), water and tillage-induced erosion

depend on different topographical parameters resulting in a specific spatial signature in the landscape. Tillage erosion is the most intense on landscape positions where water erosion is minimal (i.e. on convexities and in the proximity of upslope field boundaries), whereas areas of tillage deposition often coincide with areas of maximal water erosion as hollows (Govers et al., 1994; 1996; Van Oost et al., 2000).

The hydrological and sedimentological connectivity across cultivated hillslopes is to a large extent controlled by the presence of field borders and associated linear elements, such as hedges, roads, furrows and grass strips, which induce landscape fragmentation (Van Oost et al., 2000; Follain et al., 2006; Szilassi et al., 2006). Vegetated borders (e.g., grass strips, hedges and grassed waterways) can reinfiltrate surface runoff and trap sediment transported by water (Van Dijk et al., 1996; Caubel et al., 2003; Evrard et al., 2008). In contrast, concave anthropogenic features (e.g., furrows) provide preferential drainage pathways, thereby increasing hydrological and sedimentological connectivity across the landscape. Linear landscape elements with a compacted surface (e.g. roads, land tracks) have a limited infiltration capacity and then enhance runoff and hydrological connectivity (Wemple et al., 1996; Forman and Alexander, 1998). In tilled fields, all types of field borders act as lines of zero-flux (Dabney et al., 1999; Van Oost et al., 2000). Consequently, tillage-induced deposition and erosion preferentially occur upslope and downslope of field borders that are oriented parallel to contour lines.

Field borders can therefore act as barriers to water and sediment fluxes generated by both water and tillage erosion (Dabney et al., 1999; Govers et al., 1999; De Alba, 2003; Van Dijk et al., 2005; Knapen et al., 2008). Interaction between erosion and deposition processes at the vicinity of field borders leads to the development of anthropogenic linear landforms of several metres width (e.g., ridges-and-furrows, headlands, and lynchets). These features are common in the agricultural landscapes of western Europe (Callot, 1980; Hooke, 1988;

Zadora-Rio, 1991). These landforms are not conserved after the removal of the field border but will instead keep evolving, and may finally lead to the formation of undulations (Houben, 2008; Chartin et al., 2011). Assessing the effect of field borders and their potential removal is then essential to understand past, present and future spatial patterns of soil redistribution and soil properties in the current global change context.

Agricultural policy and mechanisation led to the massive removal of field borders through the implementation of numerous land consolidation schemes between 1960 and 1990 in western Europe (Baudry and Burel, 1984; Vitikainen, 2004), and is still ongoing in some regions. The use of ^{137}Cs-technique can therefore offer a solution to evaluate soil redistribution over these last decades (e.g., Rogowski and Tamura, 1965; Ritchie and McHenry, 1990; Walling and Quine, 1992).

This study aims to quantify and improve our understanding of the effects of land consolidation and field borders on mid-term soil erosion and on agricultural landscape evolution. In order to achieve this objective, we analysed spatial patterns of ^{137}Cs inventories for an agricultural hillslope that was subjected to land consolidation. The study area is representative for field consolidation in intensively cultivated areas of the southwestern Parisian basin (France). We used a spatially-distributed model to convert these observations into soil redistribution rates. Emphasis will be put on the impact of small-scale topographical features, especially lynchets and undulations landforms associated with local soil accumulation along current and former field borders. Finally, we discuss the wider implications of our findings in relation to agricultural landscape evolution and model development.

2. Materials and methods

2.1. Study area

2.1.1. Location and physiographical settings

The study was conducted on a 3.7 ha field located at the downslope part of a south-east facing hillslope in the southwestern Parisian Basin, France (47°08.31'N, 0°10.97'E) (Fig. 1). The area is part of the Quincampoix watershed and is characterised by an undulating topography commonly observed in terrains underlain by Cretaceous chalks in this region. In the study field, the elevation ranges between 43 to 60m with slope between 0 to 8.8%. Two types of linear anthropogenic landforms - lynchet and undulation – were also identified within this field (see further).

Soils are calcaric Cambisols, epileptic calcaric Cambisols and colluvic Cambisols with clay and loam textures (Boutin et al., 1990; FAO, 1998). The mean annual precipitation reaches ca. 600 mm and isevenly distributed throughout the year.

We reconstructed the changes in field boundaries using aerial photographs for 1945, 1959 and 2009. The study area is presently a unique field but it was divided into seven individual fields before the last important campaign of land consolidation that occurred in 1967 (Fig. 2). Interviews with local farmers and aerial photographs have demonstrated that this area has been cultivated with cereals and oilseed crops (maize, sunflower, wheat, barley and rape) since at least 1945.

2.1.2. Characteristics of the anthropogenic linear landforms

We observed one lynchet (L1) and two undulations (U1, U2) in the study area. Locations of the field borders associated with these linear landforms are presented in Figure 2. The lynchet L1 and undulations U1 and U2 are oriented perpendicularly to the steepest slope and separated by mostly regular hillslope sections in the study area (Chartin et al., 2011).

Lynchet landforms, also known as terraces, soil banks, or locally as "rideaux" in northern France and Belgium, are predominantly shaped by the progressive accumulation of

soil material upslope of a field border (Bollinne, 1971; Papendick and Miller, 1977; Van Dijk et al., 2005; Salvador-Blanes et al., 2006; Follain et al., 2007). A lynchet is defined by two morphological components separated by a field border, i.e., the axis (Fig. 3a). Uphill, progressive slope gentling from up- to downslope shapes a wide concave area (from 15 to 30m width in this region). Downhill, there is a break-in-slope that in this specific case, is 2 to 5 m-wide and reaches more than 2 m height creating a sharp discontinuity in the landscape. The soil accumulation in a lynchet evolves as a pseudo right-angle triangle (Fig. 3c).

An undulation consists of a wide gentle central convexity gradually connected by slight external concavities to the general hillslope morphology (Fig. 3b). The top of the convexity - considered as its axis - coincides closely with a former field border (Houben, 2008; Chartin et al., 2011). Undulation landforms correspond to a more or less thickened soil with a lenticular convex shape (Fig. 3d).

2.2. Topographical data

A 2 m resolution raster DEM was built from LIDAR data with the following method. Raw, tiled LIDAR datasets for the study area were assembled. Only the datasets identified as ground floor points were kept for this study (vegetation and infrastructure top points were not considered). The 2 m cells covering the area contained from 0 to 247 LIDAR points with different Z values. The median Z value was attributed to each cell centroid for cells with points whereas centroids for cells without points where deleted. Only elevation points of each cell belonging to the same landuse as the controid were used to calculate this median value. This prevents from an artificial smoothing of sharp topographic discontinuities such as lynchet borders. A triangular irregular network (TIN) was then built from the remaining centroids. The TIN was then interpolated to a 2 m resolution raster. The elevation raster was

finally filtered on a plot by plot basis depending on the land use.

2.3. ^{137}Cs analysis

2.3.1. Field sampling

Sixty-eight soil cores were sampled in the field in 2009 for ^{137}Cs activity analysis. Thirteen cores were collected along each of the five transects parallel to the steepest slope and referred to as I to V in Figure 4a to cover the entire range of topographic settings observed in the area. Sample lines 1 and 2 are located in the concavity of lynchet L1; sample lines 5 and 9 are located along the axis of undulations U1 and U2, respectively, e.g. in their central convexities; lines 4, 6, 8 and 10 are located in the external concavities of the latter undulations; and, finally, sample lines 3, 7, 11, 12 and 13 are located in areas characterised by more or less regular slopes. Three additional cores (IV-1a, IV-1b and IV-1c on Figure 4b) were sampled along transect IV to detail the effect of the present field border on the recent soil redistribution over a short distance in lynchet L1 (Fig. 4b).

Soil cores with 8 cm or 10 cm external diameter were collected with a percussion drilling machine (Eijkelkamp) up to a soil depth of about 70 to 100 cm and immediately cut into sections in the field. Depending on the local soil thickness, the first section corresponded to the uppermost 20 to 40 cm of the core. Then, successive 10-cm sections were cut off until the bedrock was reached. Two of the sixty-eight soil cores (sample points IV-1a and V-8 highlighted in Fig. 4) were cut into 5-cm sections to detail the vertical distribution of ^{137}Cs at particular locations. The V-8 soil core was collected on the downslope external concavity of undulation U2, e.g. just downslope of a former field border that was removed in 1967. Core IV-1a was sampled on the gentle slope of L1 lynchet, 3 m upslope of the present lower field-border. Each section of the 68 cores was oven-dried for 48 h at 40 °C, sieved to 8-mm. Soil in the study area contains large quantities of coarser grains and chalk fragments. Attention was

paid to collect the fine particle fraction deposited on the surface of those coarser grains. The <8mm fraction was ground to a fine powder. For each sample, a representative subsample of the <8mm fraction (approx.. 70 g) was then collected to measure ^{137}Cs activities.

2.3.2. Measuring ^{137}Cs activities

^{137}Cs in the soil cores was measured at 661 keV using low background Germanium gamma-ray detectors (Germanium hyperpure – GeHP, N-type, coaxial model) for 24 to 48 h. An initial qualitative assessment was performed on successive subsamples of each core to determine the maximum depth of the ^{137}Cs signal. The ^{137}Cs activity (A_i in Bq.kg^{-1}) was then derived for each core section. Finally, the ^{137}Cs total inventory (A_{surf} ; Bq.m^{-2}) of each core was calculated according to Eq. (1) (Sutherland, 1992).

$$A_{surf} = \sum_{i=1}^{n}\left(A_i \times \frac{M_i}{S} \right) \quad (1),$$

where A_i is the ^{137}Cs activity in the successive sections of the core (Bq.kg^{-1}); M_i is the mass (kg) of the <8 mm soil fraction of the ith sampled section; S is the surface area (m^2) of the soil core cylinder, n the total number of sampled sections sections of the core.

To estimate whether soil erosion or deposition occurred in the investigated field since the beginning of ^{137}Cs fallout (1954), ^{137}Cs inventories were compared to the local reference inventory. This latter was the mean inventory obtained in four cores sampled in neighbouring undisturbed sites such as orchards and pastures. Then, ^{137}Cs residuals were calculated according to Eq. (2):

$$Cs_{res,x} = A_{surf,x} - A_{surf,ref} \quad (2),$$

where $Cs_{res,x}$ are the ^{137}Cs residuals at the *x* core location (Bq.m^{-2}), $A_{surf,x}$ is the ^{137}Cs total inventory at the the *x* core location (Bq.m^{-2}), and $A_{surf,ref}$ is the Cs reference inventory (Bq.m^{-2}).

225 Negative residuals mean that the concerned location has underwent net soil erosion since
226 1954, whereas positive residuals indicate the occurrence of net soil deposition.
227
228 *2.4 Converting ^{137}Cs activities into erosion-deposition rates*
229 *2.4.1. Conversion model description*
230 We used a spatially explicit model to convert ^{137}Cs residuals into soil erosion and
231 deposition rates (Mg.ha^{-1}.yr^{-1} or mm.yr^{-1}). The model consists in a combination of a punctual
232 mass-balance model and a spatially distributed and process-based model of water and erosion
233 tillage processes (Van Oost et al, 2003). The mass-balance model includes both the annual
234 fallouts and susceptible losses of ^{137}Cs due to runoff (before its incorporation within the tilled
235 layer) during the whole period of the radionuclide fallout (Quine, 1995). The conversion
236 model exploits the different patterns of water and tillage erosion in a spatial analysis of ^{137}Cs
237 inventories to assess the relative contribution of water and tillage erosion processes.
238 The water-induced processes of soil erosion (rill and interrill erosion) are defined as a
239 power function of slope gradient and contributing area, following Eqs. (3) and (4):

240 $$E_{rill} = k_1 \rho_b S^a A^b , \qquad (3)$$

241 $$E_{irill} = c \rho_b S^d , \qquad (4)$$

242 where E_{rill} and E_{irll} are rill and interrill potentials, respectively (kg.m^{-2}), ρ_b is the dry bulk
243 density of the soil (kg.m^{-3}), S is the slope (m.m^{-1}), A is the contributing area per unit contour
244 width (m^2.m^{-1}), and k_1, a, b, c and d are coefficients (-).
245 The local rate of soil erosion is then calculated as the summation of both potentials for rill and
246 interrill erosion unless the local transport capacity is exceeded. The transport capacity on a
247 given slope segment is then considered as being proportional to the potential for rill erosion
248 (e.g., Desmet and Govers, 1995), Eq. (5):

249 $$T_c = k_2 E_{rill} , \qquad (5)$$

where T_c is the transport capacity ($kg.m^{-1}$) and k_2 is a coefficient (m).

When local sediment inflow exceeds the transport capacity T_c, deposition occurs. The amount of soil translocated is then equal to T_c.

The net soil flux induced by tillage translocation on a hilllsope of infinitesimal length and unit width is considered as proportional to the local slope gradient (Govers et al., 1994; Van Oost et al., 2000), Eq. (6):

$$Q_t = k_3 S = -k_3 \frac{dh}{dx}, \quad (6)$$

where Q_t represents the net downslope flux due to tillage ($kg.m^{-1}.a^{-1}$), k_3 is the tillage transport coefficient ($kg.m^{-1}.a^{-1}$), S is the local slope gradient ($m.m^{-1}$), h is the height at a given point of the hillslope (m), and x is the horizontal distance (m).

The local intensity of tillage-induced erosion (E_t in $kg.m^{-2}$) is then modelled as a diffusive process controlled by slope gradient changes, according to Eq. (7):

$$E_t = \rho_b \frac{dh}{dt} = -\frac{dQ_t}{dx} = \frac{d^2h}{d^2t}, \quad (7)$$

where t is the time (s).

Finally, field borders were considered as lines of zero flux. This means that no soil material is translocated from one field to another during tillage.

2.4.2. Conversion model application

The simulation process is iterative, and each iteration corresponds to one year. Annual ^{137}Cs fallouts used in the model were based on the measured annual fallout for the northern hemisphere (Cambrai et al., 1989). This value was rescaled to the local reference inventory using the factor α (-), Eq. (8):

$$\alpha = \frac{A_{surf,ref}}{A_{surf,NH}}, \quad (8)$$

where $A_{surf,ref}$ is the Cs reference inventory ($Bq.m^{-2}$) for the study area and $A_{surf,NH}$ is the mean Cs reference inventory ($Bq.m^{-2}$) for the northern hemisphere.

^{137}Cs fallouts associated with the Chernobyl accident were reported to be negligible in the study area and were therefore not considered in Cs reference inventories of Eq. (8) (Fourmont, 2001).

The parameter values proposed by Quine (1997) were used for the punctual mass-balance model. No a-priori assumptions were made about rates of water and tillage erosion. A specific procedure developed by Van Oost et al. (2003) and based on the Generalized Likelihood Uncertainty Estimation (Beven and Binley, 1992) was implemented to explore the parameter space for which the model was in close agreement with the observed ^{137}Cs inventories. Value ranges for parameters k_1, k_2 and k_3 (Eqs. 2, 4 and 5) used in this procedure are presented in Table 1. Coefficients a, b and d (Eqs. 2 and 3) were based on studies carried out by Desmet and Govers (1995, 1997), Van Oost et al (2000) and Van Rompaey et al. (2001).

The conversion model was applied to compare simulated and observed ^{137}Cs patterns for 3000 randomly choosen parameter sets k_1, k_2 and k_3 over the whole study area. The observational dataset used in the evaluation procedure, called “total set”, contains 67 sampling points: the point IV-1b was excluded as it is located just 1 m from point IV-1a. Likelihood values for each set of parameters were determined and associated with the corresponding model output values (Van Oost et al., 2003). The cumulative likelihood distribution of water and tillage erosion rates was then defined separately for the whole study area. From these cumulative distributions, median (M), 5^{th} (P5) and 95th (P95) percentile values were calculated to provide a quantification of model uncertainty.

3. Results and discussion

298 *3.1. Recent soil redistribution patterns and relations with topographical settings*

299 The observed ^{137}Cs reference inventory was 1367 ± 30 Bq.m^{-2} in 2009 in Seuilly (Fig.
300 5a). About 40% and 65% of the total ^{137}Cs inventory was concentrated in the uppermost 5 cm
301 and 10 cm, respectively. As observed at many other undisturbed locations, the ^{137}Cs content
302 declined almost exponentially with soil depth in these profiles (Walling and Quine, 1992).

303 The ^{137}Cs residuals (Eq. 2) ranged from -1030 Bq.m^{-2} to 980 Bq.m^{-2} in the 68 analysed
304 cores. The largest variations were observed along the steepest slope direction (NNW-SSE)
305 and were strongly affected by anthropogenic undulations U1, U2, and lynchet L1 (Fig. 6).
306 About 50% of the ^{137}Cs contained in the soil at the time of sampling (2009) originates from
307 the period between1962 and 1964. Consequently, currently observed patterns mostly reflected
308 the soil redistribution that occurred after the 1967 land consolidation, when field borders
309 associated with undulations U1 and U2 were removed (Fig. 2).

310 The ^{137}Cs residuals measured on undulation central convexities (sample lines 5 and 9)
311 ranged from -320 Bq.m^{-2} to 20 Bq.m^{-2} and were mostly negative, whereas residuals measured
312 on undulation external concavities (sample lines 4, 6, 8 and 10) ranged from 30 Bq.m^{-2} to
313 more than 730 Bq.m^{-2}. These results reflected the progressive levelling of the undulation
314 landforms since the last land consolidation. These patterns of ^{137}Cs residuals were then most
315 likely induced by redistribution through tillage practice such as it leads to soil erosion in
316 convexities and soil accumulation in concavities (Govers et al., 1994; 1996; De Alba et al.,
317 2004). The profile V-8 provided an example of ^{137}Cs vertical distribution in an undulation
318 external concavity, i.e. in a depositional context ($A_{surf,}$ = 1786 Bq.m^{-2}; Fig. 5b). The ^{137}Cs
319 vertical distribution was homogeneous in the uppermost 30 cm and then declined rapidly in
320 the next five centimetres, reflecting the mixing induced by tillage operations (Kachanovski
321 and de Jong, 1984; Ritchie and McCarty, 2003). As undulation landforms initially correspond
322 to local soil accumulation induced by former field borders, their morphology in 2009

potentially derived from the levelling of two other types of anthropogenic landforms consecutive to the field border removal: i) the undulations are former lynchets as suggested by Bollinne (1971) and Houben (2008); ii) undulations are headlands created by an asymmetric accumulation of soil due to tillage translocation on both sides of the borders (Callot, 1980; Leturcq, 2008). In both cases, the morphology corresponding to current undulations in the vicinity of the former field borders shows a strong evolution.

The ^{137}Cs residuals ranged from 420 to 560 Bq.m^{-2} 16 m upslope of the lynchet L1 field border (sample line 2). This area is characterised by a particularly gentle slope that is clearly concave. In contrast, four of the five cores collected 2m upslope of same border (sample line 1) showed negative residuals ranging from -1000 Bq.m^{-2} to -250 Bq.m^{-2} (Fig.6). Fig. 7 shows that lynchet L1 (sample lines 1 and 2) was characterised by a large variability of ^{137}Cs residuals revealing the occurrence of both erosion and deposition processes. It has nevertheless mostly undergone soil accumulation since 1967. Indeed, ^{137}Cs residuals ranged from -426 Bq.m^{-2} to 946 Bq.m^{-2}, with negative values exclusively concentrated within the first 4m upslope the field border. Even though lynchets are typically developed by the progressive accumulation of soil upslope of a field border, our results reflected that soil erosion occurred along this downfield border during the period 1954-2009. This complex behaviour could be due to specific tillage practices performed along the field border. Farmers systematically end up their tillage operations by contouring the field, i.e. perpendicularly to the main up- and downslope tillage direction in the case of the upslope and downslope field borders. This operation with the mouldboard plough results in the translocation of soil to the inside of the field. This process could explain the slight local convexity observed in the first meters of the field along the lower field border (Fig. 7). Considering this short-distance variability, sampling schemes have to be carefully designed to describe in an appropriate way

347 the major soil redistribution processes (erosion or deposition) occurring in landforms
348 associated with field borders.
349 A depositional context was also observed 10 m downslope of the current upslope field
350 border (^{137}Cs residuals varied from 475 Bq.m^{-2} to 800 Bq.m^{-2} along the sampling line 13; Fig.
351 5). Indeed, soil is thicker at this location than in surrounding areas with a depth locally up to
352 80 cm (Chartin, 2011). Moreover, the local slope is convex in the direction of the steepest
353 slope. Here again, tillage practices performed along this field border could explain the local
354 soil accumulation and the topographical convex settings. Unfortunately, sampling density was
355 not sufficient to check the relevance of this hypothesis in this specific study case.
356 Finally, spatial patterns of ^{137}Cs residuals in undifferentiated areas are rather complex
357 and do not seem to be directly influenced by slope gradient nor curvature (Fig. 6).
358
359 *3.2. Modelling erosion and deposition rates from 1954 to 2009*
360 *3.2.1. Conversion results*
361 The factor α used to determine mean annual ^{137}Cs fallouts in this area was 0.786
362 (Eq. 7). Fig. 8 presents the simulated optimal ^{137}Cs inventories, tillage and water erosion
363 simulated by the model over the whole study area.
364 The major observed patterns of ^{137}Cs inventories related to lynchets and undulations
365 were reproduced by the simulations. Convex landforms were characterised by soils with low
366 ^{137}Cs inventories when compared to the higher inventories simulated on concave landforms
367 (Fig. 8a). Tillage was found to be the dominant process controlling ^{137}Cs patterns since the
368 1967 land consolidation. Tillage erosion rates were often higher than 6 Mg.ha^{-1}.yr^{-1} and
369 reached locally up to 15 Mg.ha^{-1}.yr^{-1} in central convex parts of U1and U2 (Fig.8b). Soil
370 accumulation by tillage observed in external concave areas of undulations and over the whole
371 area of lynchet L1 seemed to be correctly reproduced with a maximum deposition rate

372 reaching 22 $Mg.ha^{-1}.yr^{-1}$. Water erosion output patterns were also greatly influenced by
373 undulation and lynchet landforms (Fig. 8c). U1 and U2 subdivided the study field in three
374 areas characterised by similar patterns of simulated water erosion. In each area, erosion of soil
375 material was simulated over most of the upslope part whereas deposition was simulated in the
376 concave depositional settings located downslope of the area. Maximum soil erosion and
377 deposition rates by water were simulated in the lower area, i.e. between U1 and L1, where the
378 general slope is the steepest. Here, erosion rates reached 0.6 $Mg.ha^{-1}.yr^{-1}$ within the U1
379 external concavity and net deposition reached 5 $Mg.ha^{-1}.yr^{-1}$ within L1 concavity.
380 Simulated tillage erosion was an order of magnitude higher than water erosion in both
381 erosional and depositional areas (e.g., the median water erosion rates was -0.20 $Mg.ha^{-1}.yr^{-1}$
382 whereas the median tillage erosion rate was -4.50 $Mg.ha^{-1}.yr^{-1}$; Tab. 2). The mean tillage
383 erosion rate over the whole study area was three to four times lower than the maximum
384 erosion rates simulated in undulations (Tab. 2; Fig. 8b). Considering the mean tillage
385 deposition rate over the whole study area, it was more than four times lower than maximum
386 deposition rates simulated within the lynchet L1 (Tab. 2; Fig. 8b). The uncertainty associated
387 with simulated water erosion and deposition was much higher than the one associated with
388 tillage simulation. This could be explained by the dominance of tillage erosion process (Tab.
389 2). Moreover, deposition rates and patterns of water erosion are largely controlled by k_2
390 whereas tillage process simulations are characterised by soil redistribution patterns that
391 remained stable for the entire range of the tested k_3 values (Van Oost et al., 2003).
392 The model runs confirmed our observations: soil redistribution by tillage is dominant
393 in the area since 1967. Tillage redistributes sediment in fields whereas water exports it from
394 fields. In this context, we estimated here that 98.5 % of the total eroded soil was deposited in
395 the study field, whereas only 1.5% was exported by water erosion. This result was in
396 agreement with previous findings obtained in the Parisian basin showing that land

consolidation generates a dramatic increase of soil redistribution within cultivated catchments, and to a slight (Evrard et al., 2010; Delmas et al., 2012) or a large increase (Boardman et al., 1994; Evrard et al., 2008) of sediment exports from the catchment, depending on the catchment topography, land use characteristics and the implementation of soil conservation measures. As soon as mechanization appeared in the 1950s, land consolidation campaigns favoured its introduction across the world and, inversely, mechanization motivated the implementation of land consolidation operations (Van Huylenbroeck et al., 1996; Crecente et al., 2002; Niroula and Thapa, 2005). However, mechanized agriculture involved higher tillage erosion rates when compared to previous non-mechanized tillage (Govers et al., 1996; Van Oost et al., 2000, 2006). Land consolidation enhances hydrological and sedimentological connectivity and leads to important increases of sediment exports in regions particularly sensitive to water erosion (Evrard et al., 2007b). However, this increase is not observed when tillage largely dominates soil redistribution. Moreover, soils developed on Cretaceous chalks appear not to be particularly sensitive to water erosion, thereby limiting the hydrological and sedimentological connectivity (Boutin et al., 1990).

Our results explicitly identified hotspot areas of soil erosion induced by land consolidation, i.e., in the vicinity of removed field borders, and hotspot areas of soil deposition, i.e. in the vicinity of present field borders and external concavities of undulations. We thereby show that land consolidation led progressively to the general levelling of the hillslope morphology. This was particularly true when considering the convex undulations. From sinks for soil material before land consolidation, the corresponding areas progressively became sources for soil material redistribution.

3.2.2. Analysis of the discrepancies

421 Even though the conversion model reproduced the major trends of soil erosion and
422 deposition recorded in the study field, observed and simulated ^{137}Cs inventories fitted rather
423 poorly ($r^2 = 0.20$, $p < 0.05$; Fig. 9). Indeed, the model tended to systematically underestimate
424 inventories in depositional settings and to overestimate inventories in highly erosive areas.
425 Simulated ^{137}Cs inventories along the linear landforms were more or less
426 underestimated (from -150 to -750 $Bq.m^{-2}$) on observed depositional settings associated with
427 lynchet L1 and undulations U1 and U2, i.e. on concave parts (lines 2, 4, 6, 8 and 10; Fig. 10a).
428 However, most of these locations were simulated as being in a depositional context (Fig. 10b).
429 Similarly, central convexities located on undulations were simulated as eroded areas. The
430 largest under-estimations (< -600 $Bq.m^{-2}$) were concentrated along the upslope field border
431 (Fig. 10a). In this case, observed depositional locations were simulated as eroded sites (Fig.
432 10b). Although deposition is simulated within a few-meter width area along this upslope
433 border (Fig. 8a), actual deposition occurring ten meters downslope of this border (along the
434 sample line 13) was not well reproduced by the model. The largest over-estimations were
435 concentrated along the downslope field-border (sample line 1 on lynchet L1) where
436 simulation errors reached up to 1000 $Bq.m^{-2}$. As mentioned before, we infer that specific
437 tillage operations performed along the upper and lower field borders could have induced
438 processes differing from the classical diffusive process associated with “infield” operations
439 and considered as the only tillage-induced process in the conversion model The mechanisms
440 of those specific processes could therefore be implemented to improve the model efficiency.
441 Furthermore, sampling could be intensified in the vicinity of the current field borders in order
442 to describe more accurately their impact on local variations of soil redistribution.
443 We therefore ran the model with a dataset (subsequently referred to as the “infield set”)
444 excluding points sampled at the vicinity of upslope and downslope field borders, i.e. sampling
445 points IV-1a, IV-1b and those located along lines 1 and 13 (n = 55). Observed and simulated

446 inventories fitted much better when using the "infield set" ($r^2 = 0.42$; $p < 0.05$; Fig. 11) than
447 when using the "total set" ($r^2 = 0.20$), but discrepancies remained.
448 Both simulations outlined that tillage-induced processes were the driving factor
449 explaining more than 95 % of the total soil redistribution that occurred after the 1967 land
450 consolidation (Table 3). We demonstrated that tillage practices levelled the field morphology,
451 and we can then hypothesise that local curvatures derived from the DEM based on the 2009
452 LIDAR data were smoothened compared to those existing in 1967. Consequently, tillage
453 erosion and deposition rates simulated for the period 1954-2009 remained necessarily under-
454 estimated when considering curvatures as the morphological parameter controlling the
455 intensity of soil translocation by this diffusive process. The more the landscape morphology
456 would have evolved since ^{137}Cs fallouts, the less the conversion of ^{137}Cs inventories into soil
457 redistribution rates would be accurate. This should be taken into account when using the ^{137}Cs
458 method to validate the parameterization of erosion models dedicated to the prediction of
459 medium-term erosion (from decades to centuries).
460
461 **4. Conclusions**
462 This study focused on the impact of land consolidation and field borders on medium
463 term soil erosion (1954-2009) and landscape morphology within a 3.7-ha field consolidated in
464 1967. The spatial patterns of ^{137}Cs inventories were analyzed and a spatially-distributed
465 conversion model simulating the respective implication of water and tillage erosion was
466 applied. The model simulated tillage erosion as the most dominant process across the study
467 area, by generating 95% of soil redistribution movements (i.e., about 4.50 $Mg.ha^{-1}.yr^{-1}$) and
468 deeply modifying the landscape morphology. Hence, soil redistribution was greatly affected
469 by the presence of current but also former field borders, where hotspots areas of erosion (on
470 undulations) and deposition (on lynchets; i.e., about 20 $Mg.ha^{-1}.yr^{-1}$) are identified. Land

consolidation contributed to the acceleration of soil redistribution within the field through the conversion of depositional areas into sediment delivering areas. The conversion model reproduced the main patterns of ^{137}Cs inventories, but simulated inventories fitted rather poorly with these latters ($r^2 = 0.20$). Discrepancies were identified and associated with sampling points located along the current field borders where tillage is performed perpendicularly to the main tillage direction in the field. This tillage operation is observed in most cultivated plots and corresponds to a contouring of the field when finishing a tillage operation. This particular tillage operation could be taken into account in a future version of the model to accurately simulate rates and patterns of past soil redistribution in fragmented cultivated hillslopes. An other outcome of this specific process is that ^{137}Cs sampling schemes have to be carefully designed to describe in an appropriate way the major soil redistribution processes occurring in landforms associated with field borders. We also suggest that the use of an accurate DEM representing the actual topography in the model leads to the underestimation of soil redistribution rates, especially in this landscape where morphology was submitted to recent and significant changes. These results have important implications for the modelling of tillage erosion and to better quantify and determine the spatial patterns of soil redistribution processes across cultivated areas in a changing environment. This is of particular interest to improve our knowledge and prediction of patterns of soil physical parameters, as carbon storage or water content, particularly sensitive to surface erosion and landscape structuration.

Acknowledgements

This project was funded by ANR (Agence Nationale de la Recherche) in the framework of the LANDSOIL project (ANR-08-VULN-006). The authors would like to gratefully thank Jean-Paul Bakyono and Isabel Pene-Galland for their role on field data collection and sample

preparation. This paper was much improved thanks to the comments of two anonymous referees. This is LSCE contribution no. X.

References

Andraski, B.J. and Lowery, B., 1992. Erosion Effects on Soil Water Storage, Plant Water Uptake, and Corn Growth. Soil Science Society of America Journal 56(6), 1911-1919.

Baudry, J., Burel, F., 1984. "Remembrement": Landscape consolidation in France. Landscape Planning 11, 235-241.

Boardman, J., Poesen, J., 2006. Soil erosion in Europe: major processes, causes and consequences. In: J. Boardman and J. Poesen (Editors), Soil erosion in Europe. Wiley, Chicester, pp. 479-489.

Berger, G., Kaechele, H. and Pfeffer, H., 2006. The greening of the European common agricultural policy by linking the European-wide obligation of set-aside with voluntary agri-environmental measures on a regional scale. Environmental Science & Policy 9(6), 509-524.

Beven, K. and Binley, A., 1992. The Future Of Distributed Models – Model Calibration And Uncertainty Prediction. Hydrological Processes 6(3), 279-298.

Boardman, J., Ligneau, L., de Roo, A., Vandaele, K., 1994. Flooding of property by runoff from agricultural land in northwestern Europe. Geomorphology 10, 183-196.

Bollinne, A., 1971. Les rideaux en Hesbaye gembloutoise - Etude morphologique et sédimentologique. Bulletin de la Société géographique de Liège 7, 61-67.

Boutin, D., Froger, D., Rassineux, J., 1990. Feuille Loudun (1724-1624), Carte des sols du Département de la Vienne et de la région Centre au 1:50000, Chambre d'Agriculture de la Vienne - IGN - INRA.

Callot, H.J., 1980. La plaine d'Alsace. Modelé agraire et parcellaire. Université de Nancy II, France.

Cambrai, R.S., Playford, K., Carpenter, R.C., 1989. Radioactive fallout in air and rain: results to the end of 1988. UK Atomic Energy Authority Report AERE-R 10155, HMSO.

Caubel, V., Grimaldi, C., Merot, P., Grimaldi, M., 2003. Influence of a hedge surrounding bottomland on seasonal soil-water movement. Hydrological Processes 17, 1811-1821.

Chaplot, V., Le Bissonnais, Y., 2003. Runoff features for interrill erosion at different rainfall intensities, slope lenghts, and gradients in agricultural loessial hillslope. Soil Science Society of America Journal 67(3), 844-851.

Chartin, C., 2011. Effet de l'évolution du parcellaire agricole sur la redistribution des sols et la morphologie des versants cultivés – exemple du Bassin parisien. Université de Tours, France, 322 pp.

Crecente, R., Alvarez, C., Fra, U. 2002. Economic, social and environmental impact of land consolidation in Galicia. Land Use Policy (19), 135-147.

Chartin, C., Bourennane H., Salvador-Blanes, S., Hinschberger, F., Macaire, J.-J., 2011. Classification and mapping of anthropogenic landforms on cultivated hillslopes using DEMs and soil thickness data — Example from the SW Parisian Basin, France. Geomorphology 135, 8-20.

Dabney, S.M., Liu, Z., Lane, M., Douglas, J., Zhu, J., Flanagan, D.C., 1999. Landscape benching from tillage erosion between grass hedges. Soil & Tillage Research 51, 219-231.

De Alba, S., 2003. Simulating long-term soil redistribution generated by different patterns of mouldboard ploughing in landscapes of complex topography. Soil and Tillage Research 71, 71–86.

De Alba, S., Lindstrom, M.J., Schumacher, T.E., Malo, D.D., 2004. Soil landscape evolution due to soil redistribution by tillage: new model of soil catena evolution in agricultural landscapes. Catena 58, 77-100.

Delmas, M., Pak, L.T., Cerdan, O., Souchère,V., Le Bissonnais, Y., Couturier, A, Sore, L., 2012. Erosion and sediment budget across scale: A case study in a catchment of the European loess belt. Journal of Hydrology 420, 255-263.

Desmet, P.J.J., Govers, G., 1995. GIS-based simulation of erosion and deposition patterns in an agricultural landscape: a comparison of model results with soil map information. Catena 25, 389-401.

Desmet, P.J.J., Govers, G., 1997. Two-dimensional modelling of the within-field variation in rill and gully geometry and location related to topography. Catena 29, 283-306.

Evrard, O., Bielders, C.L., Vandaele, K., Van Wesemael, B., 2007a. Spatial and temporal variation of muddy floods in central Belgium, off-site impacts and potential control measures. Catena 70, 443-454.

Evrard, O., Persoons, E., Vandaele, K., van Wesemael, B., 2007b. Effectiveness of erosion mitigation measures to prevent muddy floods: A case study in the Belgian loam belt. Agriculture, Ecosystems & Environment 118, 149-158.

Evrard, O., Vandaele, K., van Wesemael, B., Bielders, C.L, 2008. A grassed waterway and earthen dams to control muddy floods from a cultivated catchment of the Belgian loess belt. Geomorphology 100, 419-428.

Evrard, O., Nord, G., Cerdan, O., Souchère, V., Le Bissonnais, Y., Bonté, P., 2010. Modelling the impact of land use change and rainfall seasonality on sediment export from an agricultural catchment of the northwestern European loess belt. Agriculture, ecosystems and environment 138, 83-94.

591
592 FAO, 1998. World reference base for soil resources. Food and Agriculture Organization of
593 the United Nations. World Soil Resources Report No 84, FAO, Rome.
594
595 Follain, S., Minasny, B., McBratney, A.B., Walter, C., 2006. Simulation of soil thickness
596 evolution in a complex agricultural landscape at fine spatial and temporal scales. Geoderma
597 133, 71-86.
598
599 Forman, R.T.T., Alexander, L.E., 1998. Roads and major ecological effects. Annual Review
600 of Ecology and Systematics 29, 207-231.
601
602 Foster, G.R., 1986. Understanding ephemeral gully erosion. In: B.i.A. National Research
603 Council (Editor), Soil conservation: Assesing the national research inventory. National
604 Academy Press, Washington, pp. 90-118.
605
606 Fourmont, A., 2001. Analyse de l'évolution subactuelle des banquettes colluviales
607 anthropiques par la méthode du Césium-137. Influence sur le bilan sédimentaire du bassin du
608 Quincampoix (Sud-ouest du Bassin Parisien, France), Rapport de stage de DEA, Université
609 de Tours, France, pp. 40.
610
611 Govers, G., Lobb, D.A., Quine, T.A., 1999. Tillage erosion and translocation: emergence of a
612 new paradigm in soil erosion research. Soil & Tillage Research 51, 167-174.
613
614 Govers, G., Quine, T.A., Desmet, P.J.J., Walling, D.E., 1996. The relative contribution of soil
615 tillage and overland flow erosion to soil redistribution on agricultural land. Earth Surface
616 Processes and Landforms 21, 929-946.
617
618 Govers, G., Vandaele, K., Desmet, P.J.J., Poesen, J., Bunte, K., 1994. The role of tillage in
619 soil redistribution on hillslopes. European Journal of Soil Science 45, 469-478.
620
621 Hooke, D., 1988. Cosmogenic nuclides, topography, and the spatial variation of soil depth.
622 Geografiska Annaler 70 B(1), 123-131.
623
624 Houben, P., 2008. Scale linkage and contingency effects of field-scale and hillslope-scale
625 controls of long-term soil erosion: anthropogeomorphic sediment flux in agricultural loess
626 watersheds of Southern Germany. Geomorphology 101, 172-191.
627
628 Kachanovski, R. G., de Jong, E., 1984. Predicting the temporal relationship between soil
629 Cesium-137 and erosion rate. Journal of Environmental Quality 13(2), 301-304.
630
631 Knapen, A., Poesen, J., Govers, G., De Baets, S., 2008. The effect of conservation tillage on
632 runoff erosivity and soil erodibility during concentrated flow. Hydrological Processes 22,
633 1497-1508.
634
635 Leturcq, S., 2008. Fonction et devenir d'un réseau invisible: les crêtes de labour dans les
636 terroirs beaucerons (XIVe-XXe siècles), COST du Mans. Marqueurs des paysages et
637 systèmes socio-économiques. R.Compatangelo-Soussignan, J.R.Bertrand, J.Chapman, P.Y.
638 Laffont, Rennes (France), pp. 163-174.
639

Lindstrom, M.J., Nelson, W.W., Schumacher, T.E., 1992. Quantifying tillage erosion rates due to moldbard plowing. Soil & Tillage Research 24, 243-255.

Lindstrom, M.J., Nelson, W.W., Schumacher, T.E., Lemme, G.D., 1990. Soil movement by tillage as affected by slope. Soil & Tillage Research 17, 255-264.

Montgomery, J.A., McCool, D.K., Busacca, A.J., Frazier, B.E., 1999. Quantifying tillage translocation and deposition rates due to moldboard plowing in the Palouse region of the Pacific Northwest, USA. Soil & Tillage Research 51, 175-187.

Niroula,, G.S., Thapa, G.B. 2005. Impacts and causes of land fragmentation, and lessons learned from land consolidation in South Asia. Land use Policy 22, 358-372.

Papendick, R.I., Miller, D.E., 1977. Conservation tillage in Pacific Northwest. Journal of Soil and Water Conservation 32, 49-56.

Papiernick, S.K., Schumacher, T.E., Lobb, D.A., Lindstrom, M.J., Lieser, M.L., Eynard, A., Schumacher, J.A., 2009. Soil properties and productivity as affected by topsoil movement within an eroded landform. Soil & Tillage Research 102, 67-77.

Pimentel, D., Harvey, C., Resosudarmo, P., Sinclair, K., Kurz, D., McNair, M., Crist, S., Shpritz, L., Fitton, L., Saffouri, R., Blair, R. 1995. Environmental and economic costs of soil erosion and conservation benefits. Science 267(5201), 1117-1123.

Poesen, J., 1984. The influence of slope gradient on infiltration rate and Hortonian overland flow volume. Z. Geomorphol., N.F. Suppl.-Bd. 49, 117-131.

Quine, T.A., 1995. Estimation of erosion rates from caesium-137 data: the calibration question. In: I.D.L. Webster, A.M. Gurnell and B.W. Webb (Editors), Sediment and Water Quality in River Catchments. John Wiley & Sons, Chicester, pp. 307-329.

Quine, T.A., Govers, G., Walling, D.E., Zhang, X., Desmet, P., Zhang, Y., Vandaele, K., 1997. Erosion processes and landform evolution on agricultural land - new perspectives from caesium-137 measurements and topographic-based erosion modelling. Earth Surface Processes and Landforms 22, 799-816.

Ritchie, J.C., McCarty, G.W., 2003. Using ^{137}Cesium to understand soil carbon redistribution on agricultural watersheds. Soil and tillage Research 69, 45-51.

Ritchie, J.C., McHenry, J.R., 1990. Application of radioactive fallout Cesium-137 for measuring soil erosion and sediment accumulation rates and patterns: a review. Journal of Environmental Quality 19, 215-233.

Rogowski, A.S., Tamura, T., 1965. Movement of 137Cs by runoff, erosion and infiltration on the alluvial Captina silt loam. Health Physics 11(12), 1333-1340.

Salvador-Blanes, S., Cornu, S., Couturier, A., King, D., Macaire, J.-J., 2006. Morphological and geochemical properties of soil accumulated in hedge-induced terraces in the Massif Central, France. Soil and Tillage Research 85, 62–77.

690 Sutherland, R.A., 1992. Caesium-137 estimates of erosion in agricultural areas. Hydrological
691 Processes 6, 215-225.
692
693 Szilassi, P., Jordan, G., Van Rompaey, A., Csillag, G., 2006. Impacts of historical land use
694 changes on erosion and agricultural soil properties in the Kali Basin at the Lake Balaton,
695 Hungary. Catena 68, 96-108.
696
697 Van Dijk, P.M., Auzet, A.-V., Lemmel, M., 2005. Rapid assessment of field erosion and
698 sediment transport pathways in cultivated catchments after heavy rainfall events. Earth
699 Surface Processes and Landforms 30(2), 169-182.
700
701 Van Dijk, P.M., Kwaad, F.J.P.M., Klapwijk, M., 1996. Retention of water and sediment by
702 grass strips. Hydrological Processes 10, 1069-1080.
703
704 Van Huylenbroeck, G., Castro Coelho, J., Pinto, P.A. 1996. Evaluation of Land Consolidation
705 Projects (LCPs): A Multidisciplinary Approach. Journal of Rural Studies 12(3), 297-310.
706
707 Van Muysen, W., Govers, G., Bergkamp, G., Roxo, M., Poesen, J., 1999. Measurement and
708 modelling of the effects of initial soil conditions and slope gradient on soil translocation by
709 tillage. Soil & Tillage Research 51, 303-316.
710
711 Van Oost, K., Govers, G., De Alba, S., Quine, T.A. 2006. Tillage erosion: a review of
712 controlling factors and implications for soil quality. Progress in Phiysical geography 30(4),
713 443-466.
714
715 Van Oost, K., Govers, G., Desmet, P.J.J., 2000. Evaluating the effects of changes in landscape
716 structure on soil erosion by water and tillage. Landscape Ecology 15, 577-589.
717
718 Van Oost, K., Govers, G., Van Muysen, W., 2003. A process-based model for Caesium-137
719 derived erosion rates on agricultural land: an integrated spatial approach. Earth Surface
720 Processes and Landforms 28, 187-207.
721
722 Van Rompaey, A.J.J., Verstraeten, G., Van Oost, K., Govers, G., Poesen, J., 2001. Modelling
723 mean annual sediment yield using a distributed approach. Earth Surface Processes and
724 Landforms 26(11), 1221-1236.
725
726 Vitikainen, A., 2004. An overview of land consolidation in Europe. Nordic Journal of
727 Surveying and Real Estate Research 1, 25-44.
728
729 Walling, D.E., Quine, T.A., 1992. The use of Caesium-137 measurements in soil erosion
730 surveys, Erosion and sediment transport monitoring programmes in river basins. IAHS, Oslo,
731 pp. 143-152.
732
733 Wemple, B.C., Jones, J.A., Grant, G.E., 1996. Channel network extension by logging roads in
734 two basins, Western Cascades, Oregon. Water Resources Bulletin 32, 1195-1207.
735
736 Zadora-Rio, E., 1991. Les terroirs médiévaux dans le Nord-Ouest de l'Europe, Pour une
737 Archéologie agraire. J. Guilaine, Paris, pp. 165-192.

Table
Click here to download Table: Tables.doc

Table 1. Values of parameters and coefficients input in the model application.

Parameter / coefficient	Related to Equation	Values	
a (-)	(3)	1.45	
b (-)	(3)	0.75	
d (-)	(4)	0.8	
		Minimum	Maximum
k_1 (-)	(3)	0	0.40
k_2 (m)	(5)	20	220
k_3 ($Mg.m^{-1}.yr^{-1}$)	(6)	300	1000

Table 2. Simulated soil redistribution rates for the whole study area for the period 1954-2009. P5 and P95 are the 5th and 95th percentile simulation limits, respectively, and M the median.

	Mean erosion ($Mg.ha^{-1}.yr^{-1}$)			Mean deposition ($Mg.ha^{-1}.yr^{-1}$)		
	P5	M	P95	P5	M	P95
Water	-0.69	-0.20	-0.13	0.07	0.13	0.24
Tillage	-4.55	-4.50	-4.46	4.47	4.50	4.55

Table 3. Results of the conversion model applications to “Total” and “Infield”datasets.

Dataset	Elevation inputs	R^2	Mean erosion ($Mg.ha^{-1}.yr^{-1}$)	Mean deposition ($Mg.ha^{-1}.yr^{-1}$)	Implication of Tillage (%)
Total	LIDAR	0.20	-4.70	4.63	~ 98
Infield		0.42	-5.82	5.77	~ 98

Figure

Fig. 1. Location of the study area.

Fig. 2. Reconstruction of the field borders in 1945, 1959 and 2009.

Fig. 3. Geometrical characteristics of the two types of anthropogenic landforms, and the associated soils: (a) and (c) provide a picture and a cross-section of a lynchet; (b) and (d) provide a picture and a cross-section of an undulation.

Fig. 4. ^{137}Cs sampling schemes. (a) Sampling in the whole study area. (b) Zoom on samples to give details on lynchet L1.

Fig. 5. Vertical distribution of ^{137}Cs in: (a) mean reference profile of Seuilly, (b) profile V-8 and (c) profile IV-1a.

Fig. 6. ^{137}Cs residuals measured in the study area with slope gradient contours.

Fig. 7. ^{137}Cs residuals measured along a topographic cross-section within lynchet L1 (transect IV).

Fig. 8. Model outputs overlayed on an isometric projection of the study area topography: (a) simulated ^{137}Cs inventories, (b) simulated soil redistribution rates by tillage erosion, and (c) simulated soil redistribution rates by water erosion.

Fig. 9. Median simulated 137Cs inventories plotted against observed 137Cs inventories. Black line is the 1:1 line and grey lines correspond to the ^{137}Cs reference inventory (i.e., 1367 Bq.m-2).

Fig. 10. Spatial distribution of a) simulation errors and b) simulated ^{137}Cs residuals in the study field.

Fig. 11. Median simulated ^{137}Cs inventories, based on the “infield dataset”, plotted against observed ^{137}Cs inventories. Black line is the 1:1 line and grey lines correspond to the ^{137}Cs reference inventory (i.e., 1367 Bq.m-2).

Figure
Click here to download high resolution image

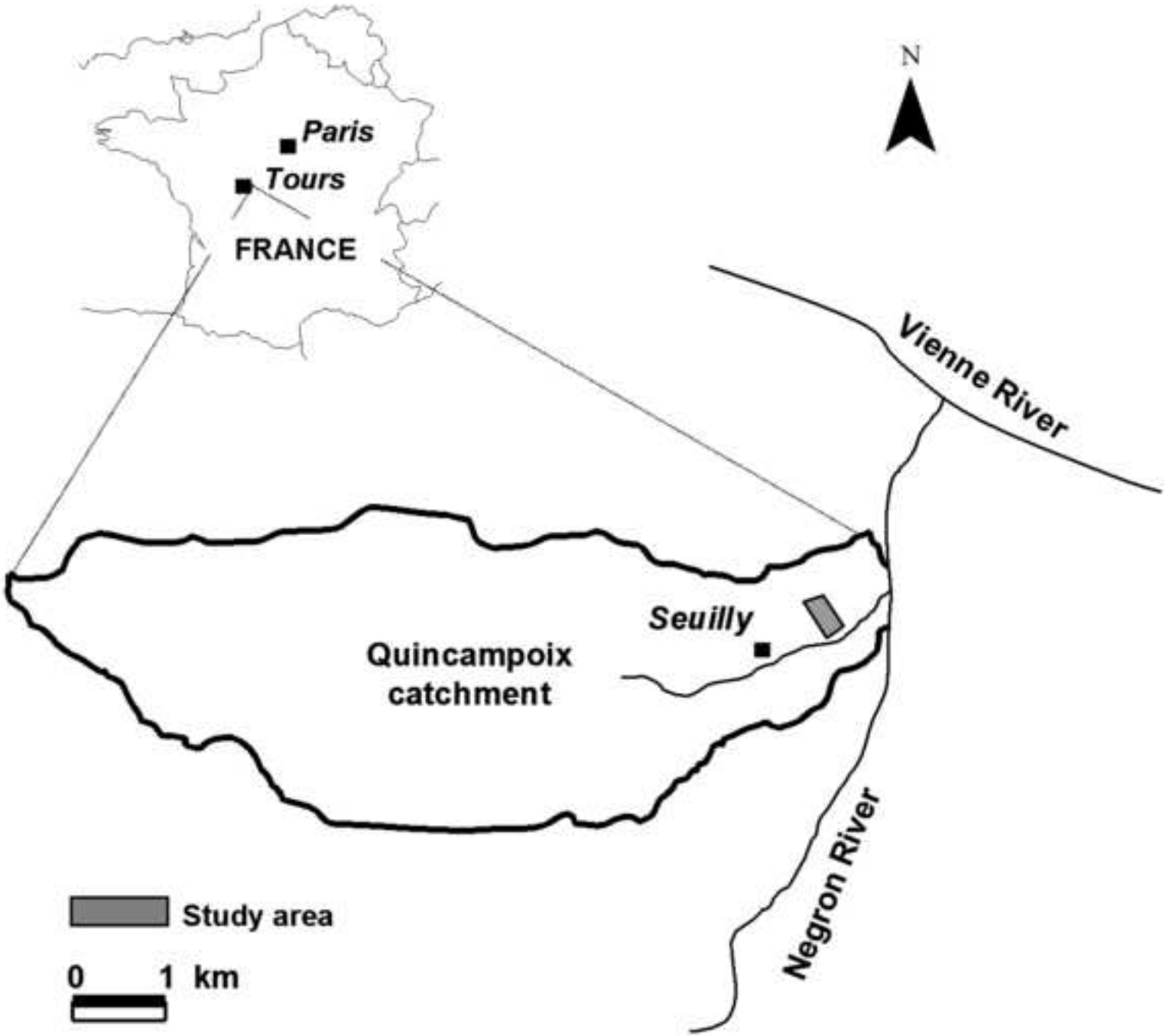

Figure

Click here to download high resolution image

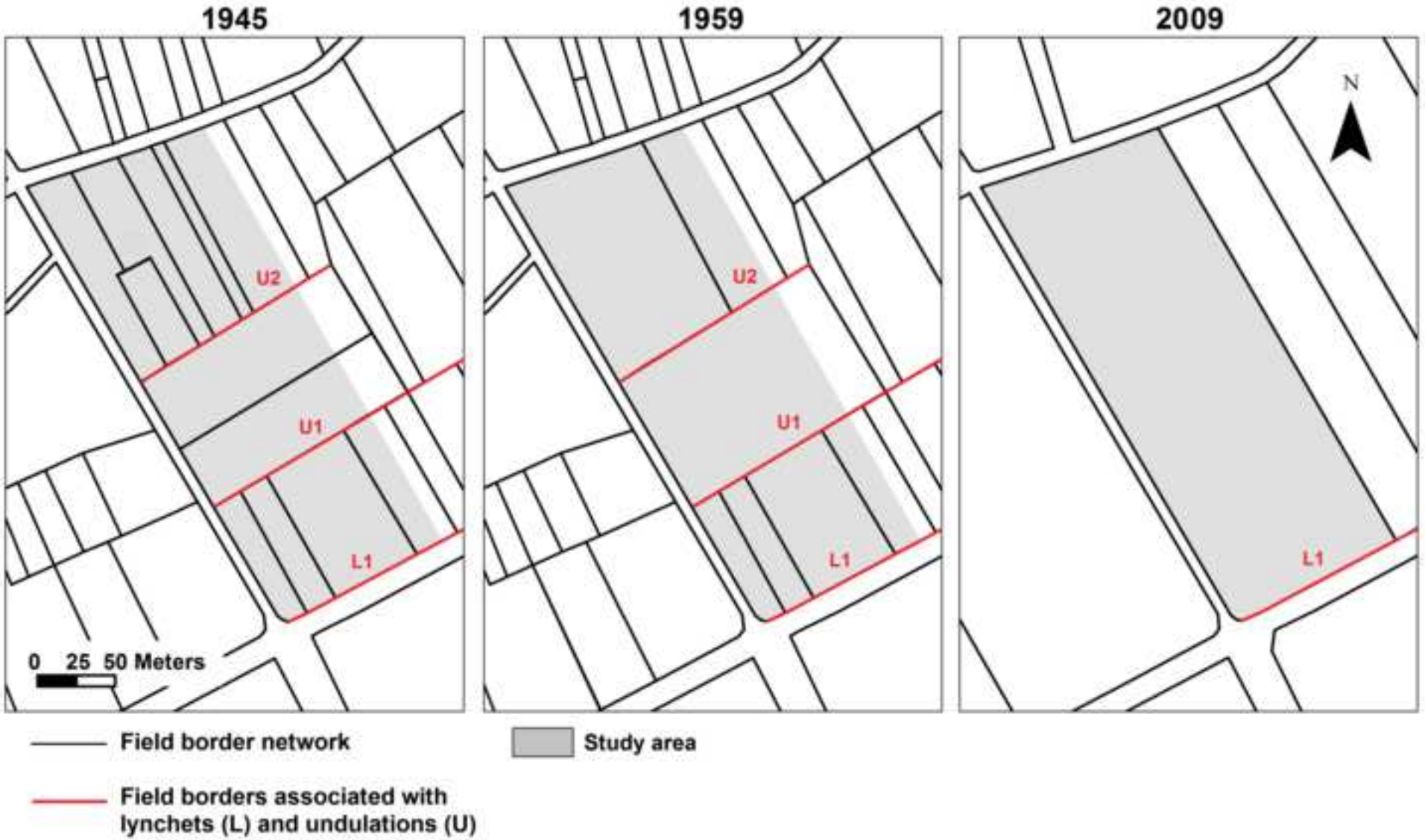

Figure

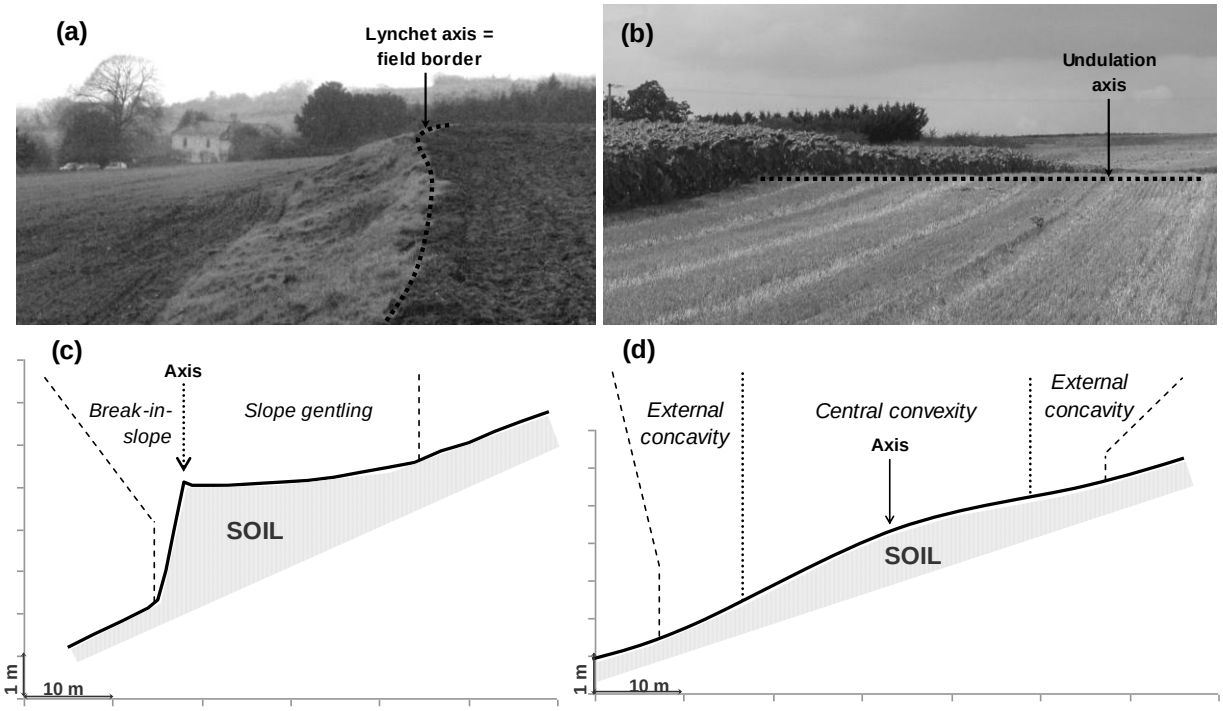
(a)
Lynchet axis = field border
(b)
Undulation axis
(c)
Axis
Break-in-slope
Slope gentling
SOIL
1 m
10 m
(d)
External concavity
Central convexity
Axis
External concavity
SOIL
1 m
10 m

Figure

Click here to download high resolution image

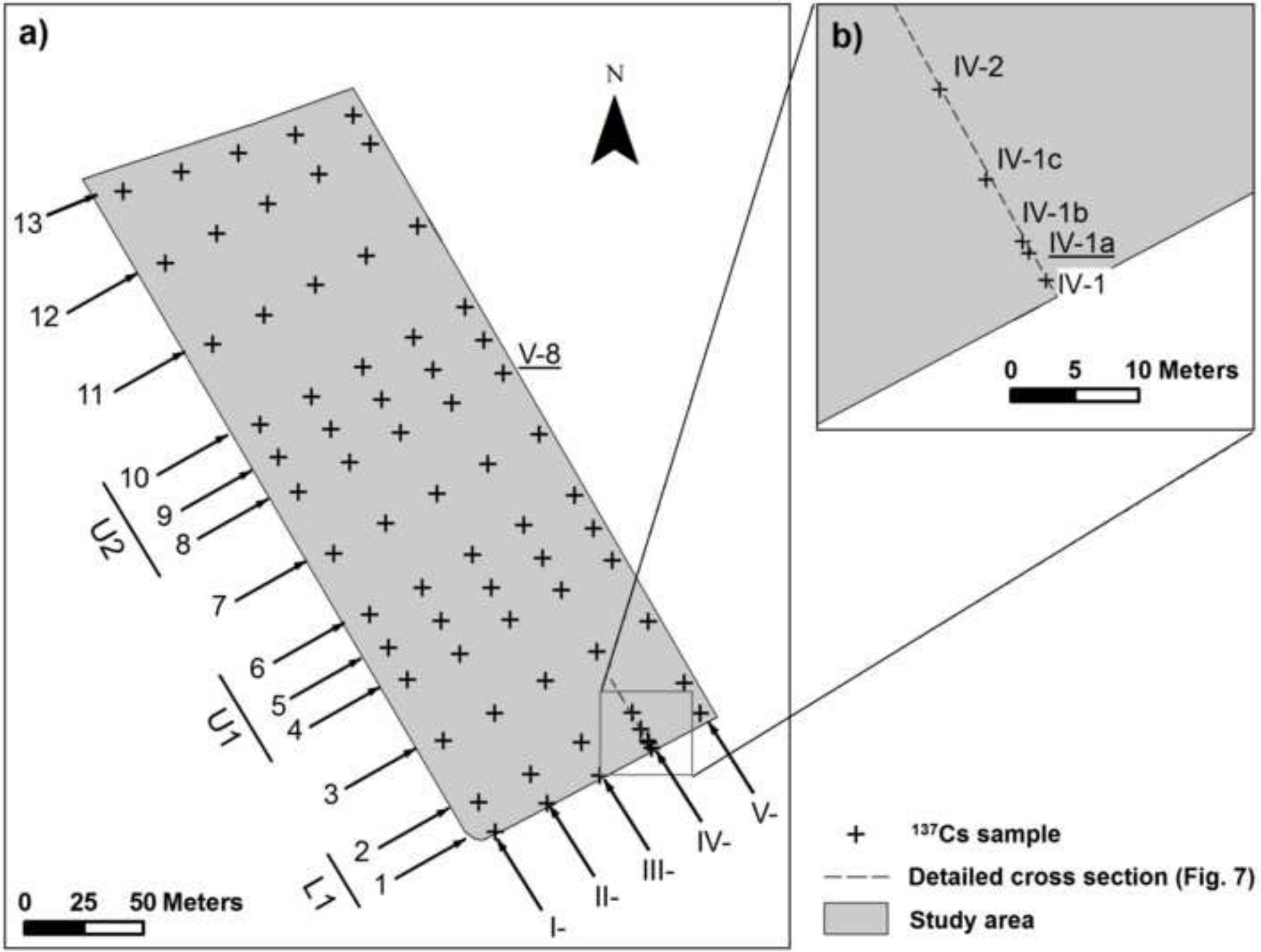

Figure

Click here to download high resolution image

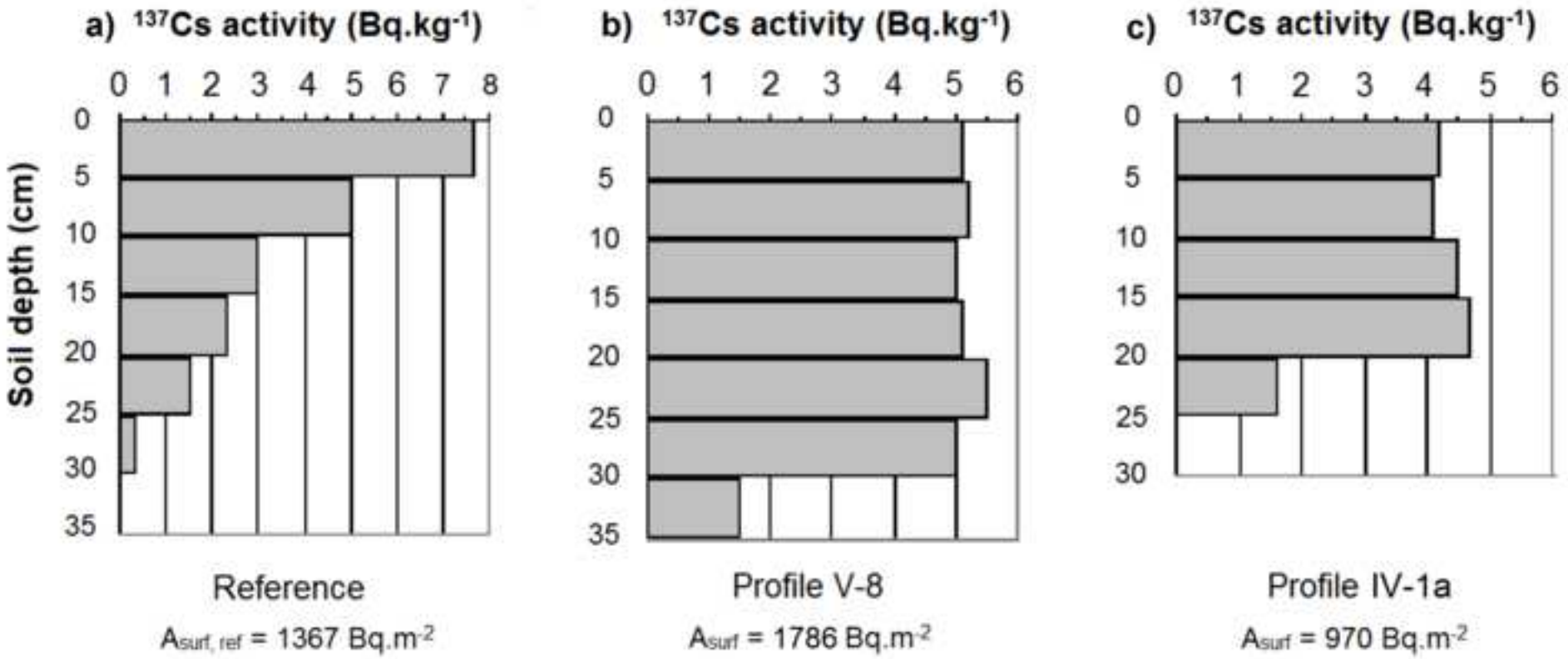

Figure

Click here to download high resolution image

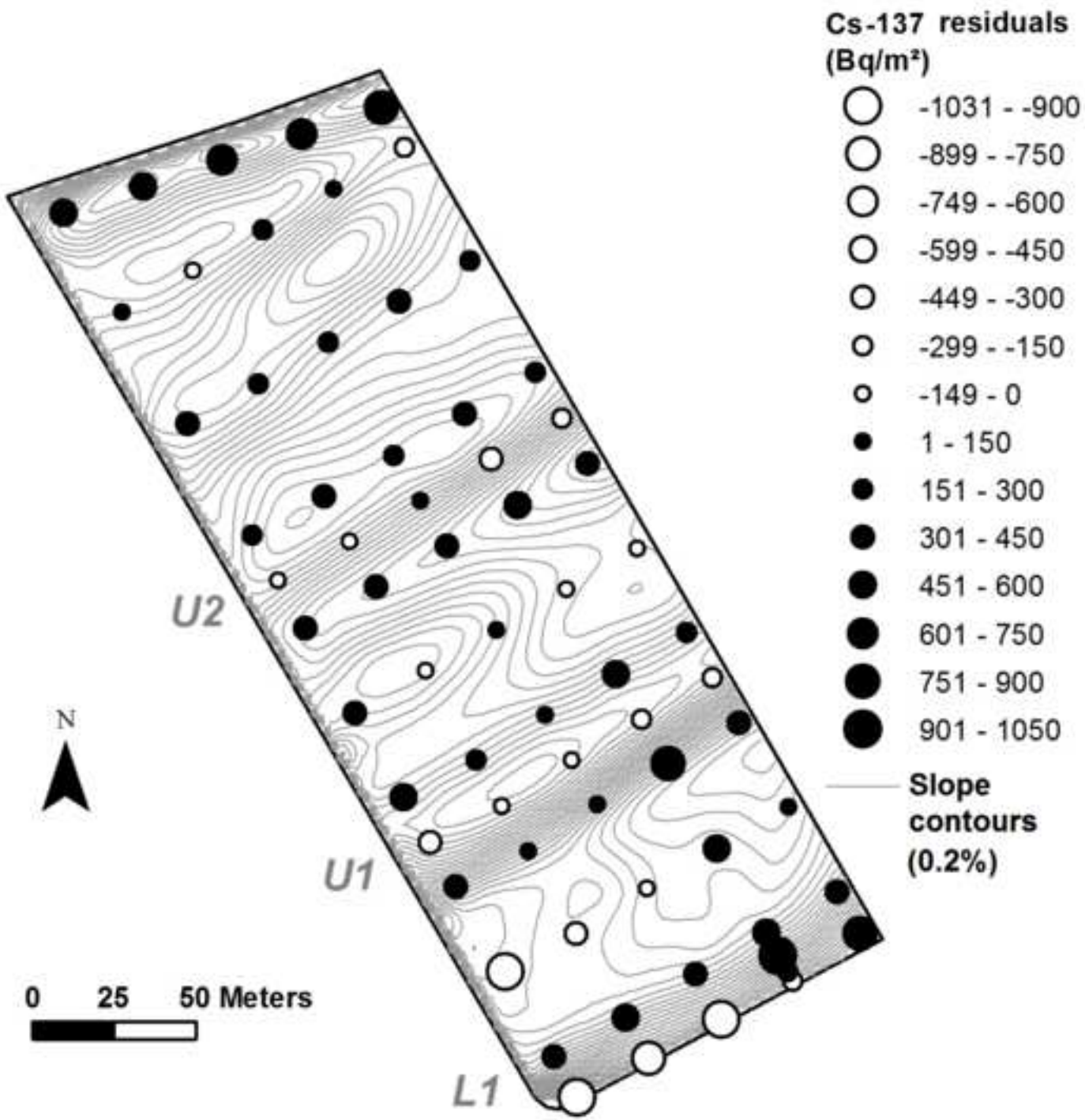

Figure

Click here to download high resolution image

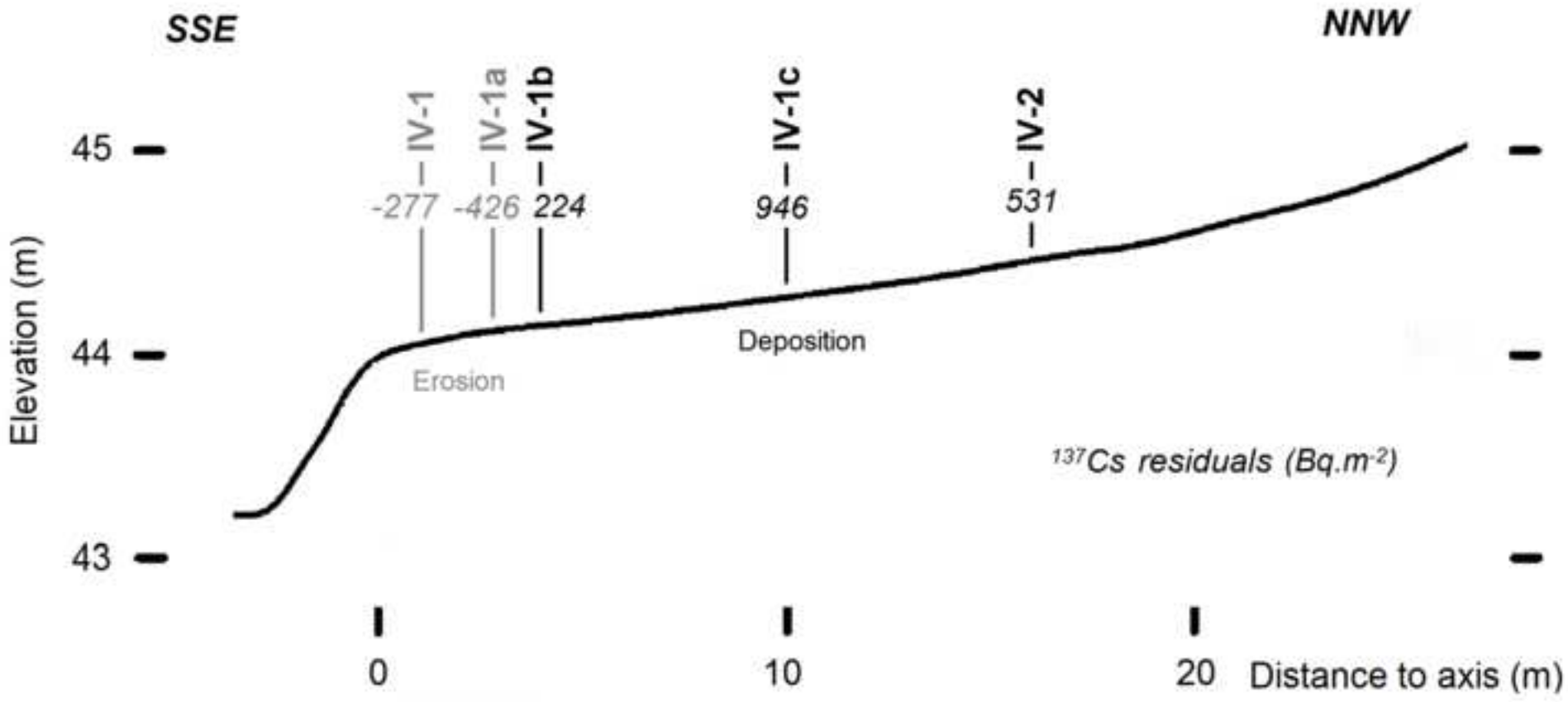

Figure

Click here to download high resolution image

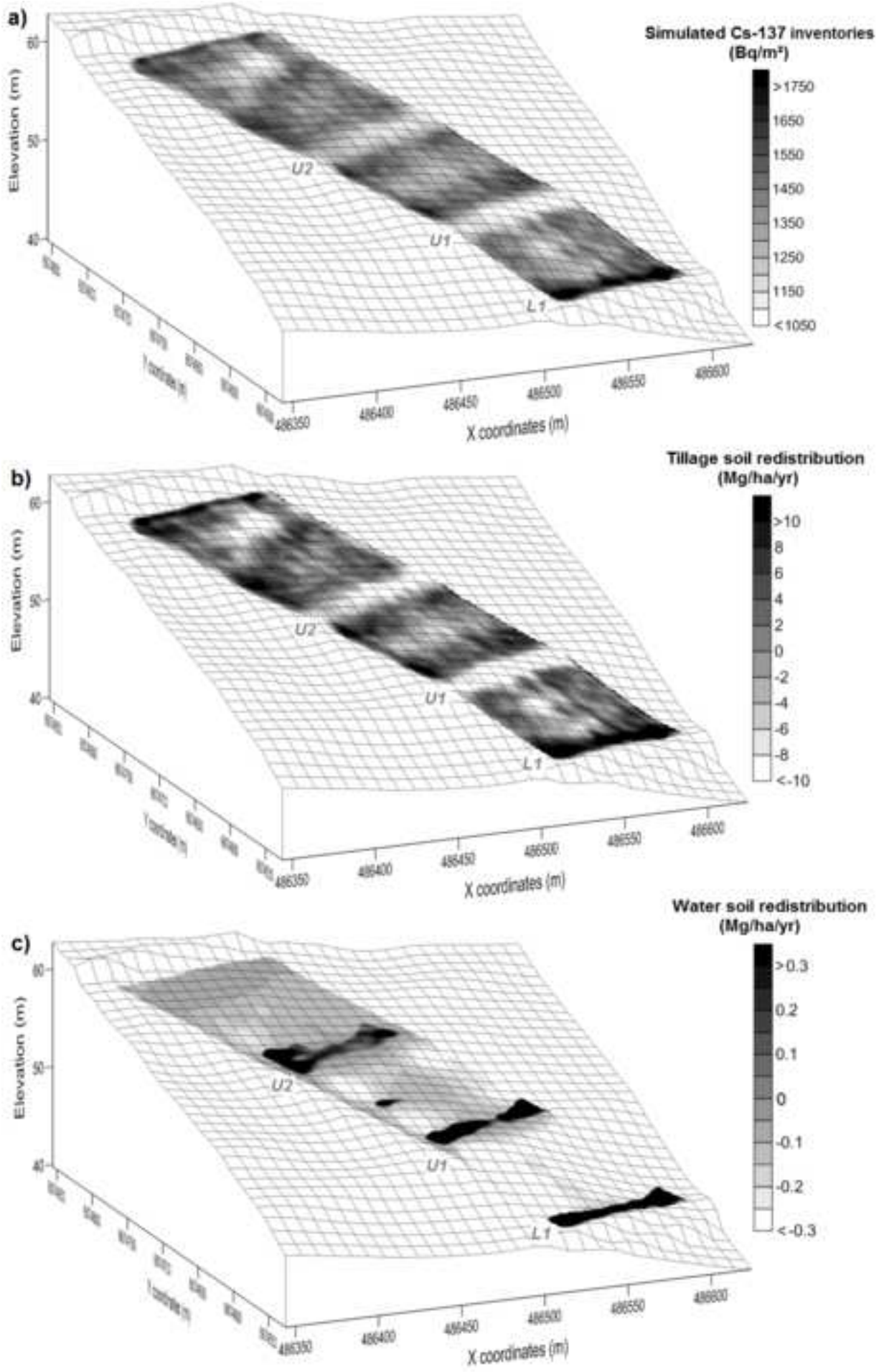

Figure
Click here to download high resolution image

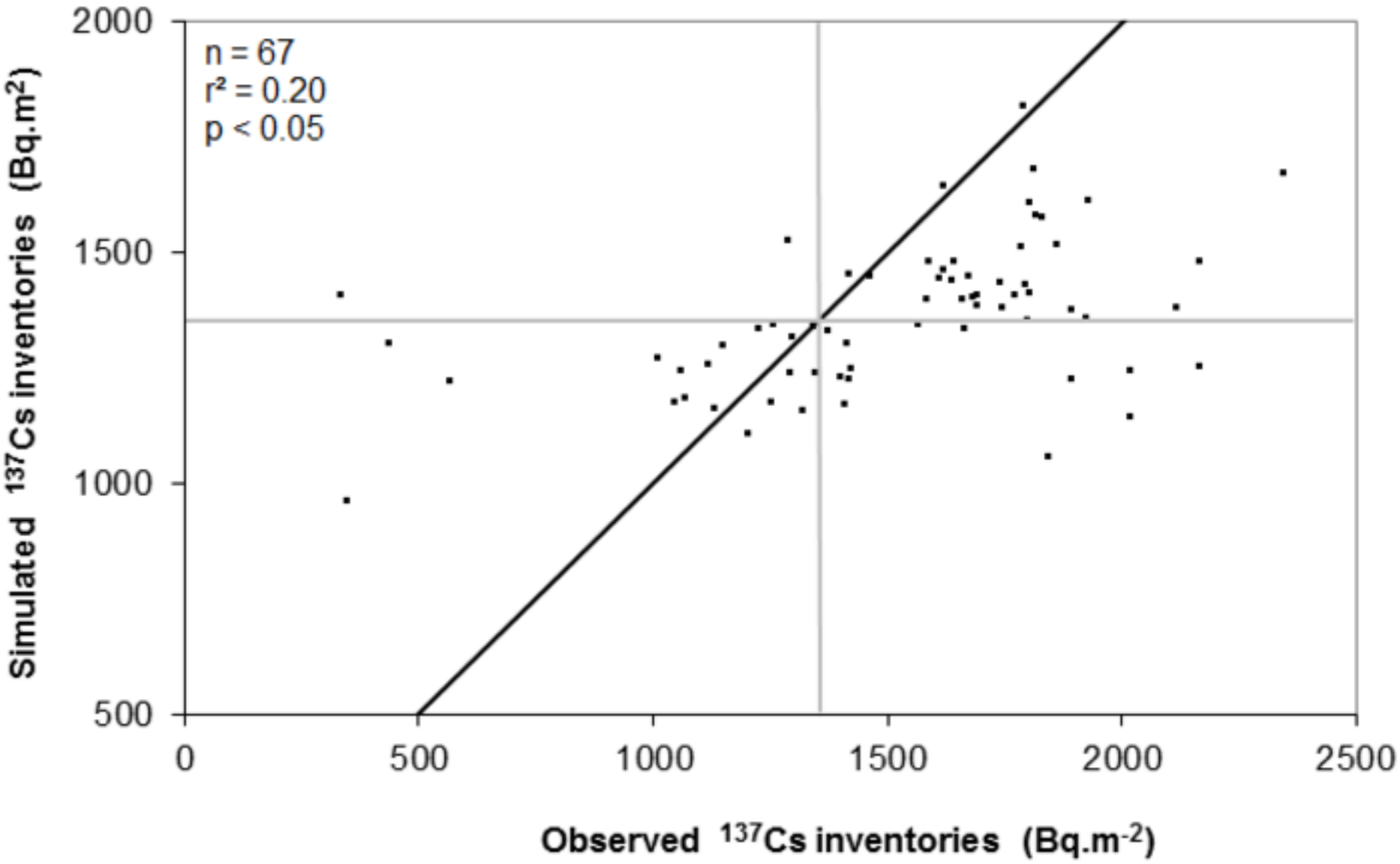

Figure
Click here to download high resolution image

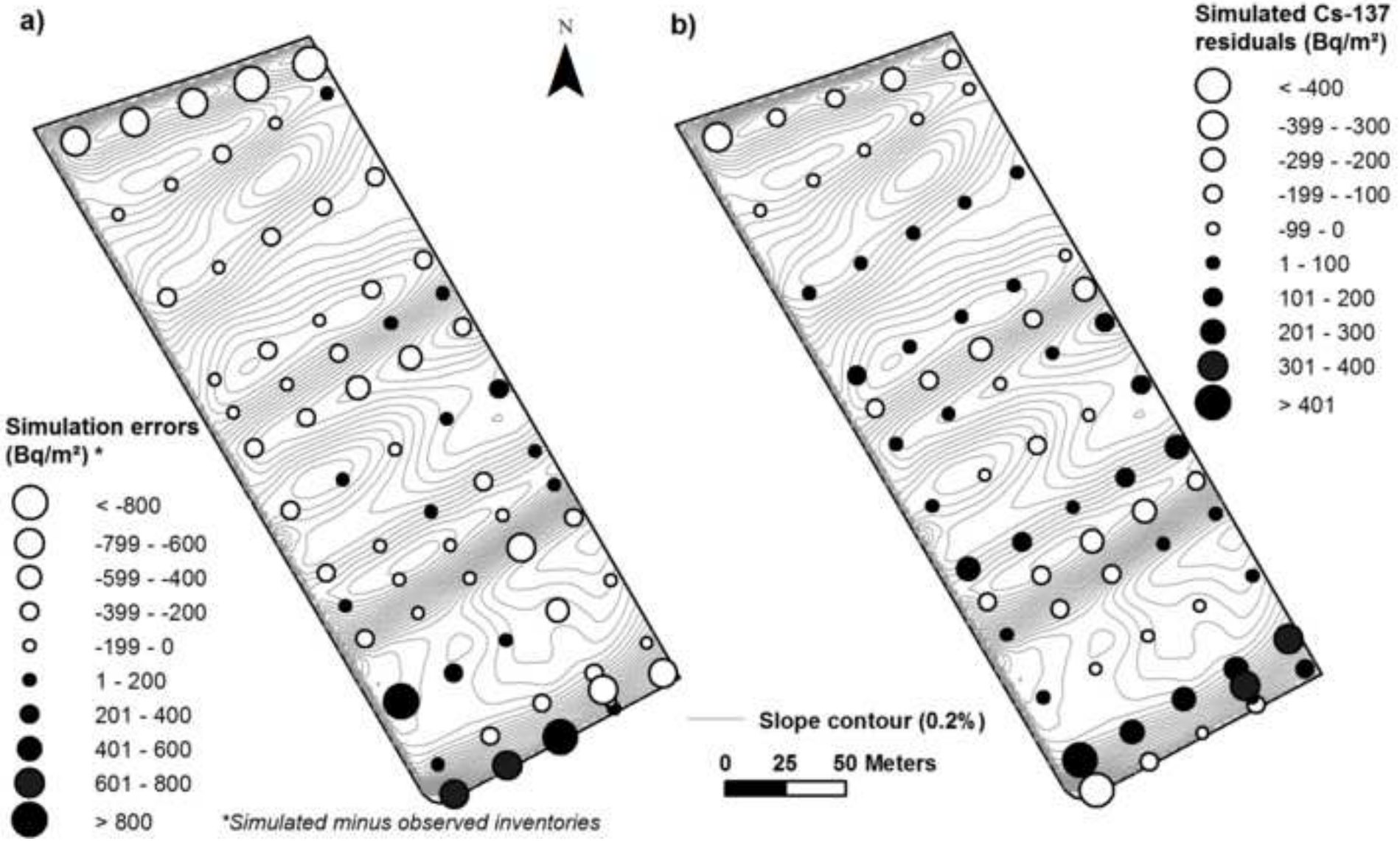

Figure

Click here to download high resolution image